European Journal of Radiology 120 (2019) 108675

Contents lists available at ScienceDirect

European Journal of Radiology

journal homepage: www.elsevier.com/locate/ejrad

Research article

Camera-based respiratory triggering improves the image quality of 3D magnetic resonance cholangiopancreatography

Felix Harder[a,1], Fabian K. Lohöfer[a,1], Georgios A. Kaissis[a,1], Christoph Zoellner[a], Omar Kamal[a,d], Christoph Katemann[b], Andreas Hock[b], Julien Senegas[b], Johannes M. Peeters[c], Ernst J. Rummeny[a], Dimitrios Karampinos[a], Rickmer F. Braren[a,*]

[a] Institute for Diagnostic and Interventional Radiology, School of Medicine of the Technical University of Munich, Ismaninger Straße 22, D-81675 Munich, Germany
[b] Philips Healthcare, Hamburg, Germany
[c] Philips Healthcare, Best, The Netherlands
[d] Department of Radiology, South Egypt Cancer Institute, Assiut University, Egypt

ARTICLE INFO

Keywords:
Diagnostic techniques and procedures
Magnetic resonance imaging
Magnetic resonance cholangiopancreatography
Biliary tract
Pancreatic ducts

ABSTRACT

Purpose: To evaluate the performance of a novel camera-based breathing navigation system in respiratory-triggered (CRT) 3D-magnetic resonance cholangiopancreatography (MRCP) at 3T MRI.

Methods: Two 3D-MRCP data sets were acquired subsequently within one imaging session with traditional respiratory belt- (BRT) or camera- (CRT) based triggering in 28 patients. Overall image quality, blurring, motion artifacts and discernibility of the pancreaticobiliary tree (PBT) structures were scored on a 4-point scale retrospectively by 2 radiologists. The contrast ratio between the common bile duct and its adjacent tissue was measured by region-of-interest (ROI) analysis. The signal intensity increase at the duct boundaries was quantified by *line profiles* to objectify blurring and motion artifacts. The extracted respiratory signal curves were analyzed for signal quality and trigger timing.

Results: Total scan time was 72 s for both acquisitions. CRT yielded significantly better ratings in image quality, background suppression, blurring and discernibility of PBT structures compared to BRT. Contrast ratios were significantly higher in CRT (0.94 ± 0.03) than in BRT (0.93 ± 0.03) exams; *paired* t test $P = 0.0017$. *Line profile* slopes through the common bile duct revealed significantly higher values in CRT (42.23 ± 8.74% of maximum intensity/mm) compared to BRT (36.06 ± 8.96% of maximum intensity/mm; *paired* t test $P < 0.0001$). Camera-derived respiratory signal curves showed a higher SNR, lower standard deviation of the signal amplitude and less incorrect triggering than the respiratory belt-derived respiratory signal curves.

Conclusion: Camera-based respiratory triggering significantly improves image quality of 3D-MRCP compared to conventional respiratory belt triggering.

1. Introduction

MRCP plays a crucial role in the detection and diagnostic work up of pathologies of the pancreatobiliary tree (PBT) [1–5]. Single shot 2D, and more recently breath-hold 3D MRCP sequences are widely applied owing to their short acquisition time [6,7]. However partial volume effect, volume averaging and reduced signal intensity can compromise the diagnostic validity in these acquisition types [1].

In contrast, higher signal intensity, with the potential for the delineation of even smallest ductal structures can be achieved by respiratory-triggered (RT) 3D MRCP [7,8]. However, higher signal intensity of free-breathing 3D MRCP sequences comes at the cost of longer acquisition times, and an increased risk for artefacts from respiratory motion, especially in patients with irregular breathing patterns [9].

Several techniques have been implemented to reduce artefacts from

Abbreviations: AUC, area under the curve; BRT, belt respiratory triggered MRCP; CBD, common bile duct; CRT, camera respiratory triggered MRCP; CS, compressed sensing; fMRI, functional magnetic resonance imaging; MIP, maximum intensity projection; MRCP, magnetic resonance cholangiopancreatography; PBT, pancreatobiliary tree; ROI, region of interest; SENSE, sensitivity encoding; SI, signal intensity

* Corresponding author.
E-mail address: rbraren@tum.de (R.F. Braren).

[1] These authors contributed equally to this work and share the first authorship.

https://doi.org/10.1016/j.ejrad.2019.108675
Received 15 May 2019; Received in revised form 12 September 2019; Accepted 17 September 2019

respiratory motion, by restricting the acquisition to the same short time window during the end-expiratory phase. These primarily include respiratory belts and navigator pulse sequence modules [1,10]. Both techniques hold severe limitations: they record motion curves for acquisition triggering from a small area of a complex moving organ despite a non-linear relationship between surface or diaphragmatic motion and organ position. In addition, the quality of navigator triggering can be reduced in patients with low liver signal (e.g. iron overload), which causes low signal difference at the diaphragm between lung and liver tissue. Regarding the use of respiratory belts, positioning can be time consuming, requires a tight fit of the belt to avoid flat or noisy signals and a change in breathing pattern (in theory) would require repositioning.

Recently, optical devices have been introduced, which deduce triggering curves by tracking surface motion [11–15], with the potential benefit of a more globally (i.e. from a larger surface area) acquired signal and no need for belt (re-)positioning. However, previous studies were mostly performed in musculoskeletal MRI or fMRI of the brain, less prone to motion artefacts compared to e.g. upper abdominal imaging.

The aim of this study was to evaluate the performance of a novel camera-based breathing navigation system in respiratory-triggered (CRT) 3D MRPC compared to conventional respiratory belt triggering.

2. Material and methods

2.1. Patient cohort

A total of 28 patients (69 ± 15.2 years, range 19–89; 15 male/13 female) were included in this prospective study. All images were acquired between January and March 2019. MRCP was performed for the following indications: pancreatitis (n = 5), focal pancreatic (n = 19) or biliary lesion (n = 4). Approval by local ethics committee (180/17S, Ethikkommission der Fakultät für Medizin der Technischen Universität München) was given. Requirement for written informed consent was waived.

2.2. Data acquisition

All MRI data sets were acquired on a latest generation 3T MR system (Philips Ingenia ElitionX; Philips Medical Systems, Best, The Netherlands). In every patient two compressed sensing-accelerated (CS factor 15) 3 dimensional (3D) MRCP sequences, using either the pressure-based respiratory belt (Invivo, Gainesville, USA)

(RBT) or the camera (VitalEye, Philips Medical Systems, Best, The Netherlands) (CBT) derived-signal, were acquired in random order. The same scan parameters were used in both sequences, as listed in Table 1. Additionally, the following sequences were acquired within the clinical routine protocol: axial and coronal 3 mm T2w, axial 4 mm DWI and axial 4 mm mDIXON dynamic. In the CBT acquisitions, a built-in-the-bore camera of type IDS uEye (IDS, Obersulm, Germany) equipped with a 4.2 mm lens (Lensation, Karlsruhe, Germany) was used to acquire video data of the subject torso during MR image acquisition. The camera was operated at 20 frames per second. Breathing signals were derived in real-time from the video data using a fully automated algorithm developed previously for patient monitoring and streamed to the MR data acquisition system via the scanner physiology interface [16]. This allowed the acquisition of breathing signals simultaneously with both the respiratory belt and the above described optical sensor, that were stored during scanning in physiology log-files for further analysis

Table 1
3D MRCP scan parameters for both sequences.

CS acceleration factor	15
Acquisition time (s)	72
FOV (mm) FH/RL/AP	280/280/80
Acquisition voxel size (mm) FH/RL/AP	1.09/1.10/2.00
Reconstruction voxel size (mm) FH/RL/AP	0.73/0.73/1.00
Fast imaging mode	TSE
TE_{eff}/TE_{equiv} (ms)	480/427
Act. TR (ms)	1418
Act. TE (ms)	480
Flip angle (°)	90
Fat suppression	SPIR
Receiver bandwidth (Hz/pixel)	224
TSE factor	90

2.3. Qualitative image analysis

Qualitative image analysis was performed by two radiologists with 6 (F.L.) and 2 (F.H) years of experience.

Images were provided as 3 plane multiplanar reformations (MPR) from CRT and BRT MRCP (slice thickness: 2 mm), coronal thin slab MIP (slice thickness/increment 4/2 mm) and MIP-based 3D-surface-renderings. Qualitative image analysis was based on a 4-point Likert scale. Overall image quality (IQ) was rated as 1 = poor; 2 = fair; 3 = good; 4 = excellent. Blurring and motion artefacts were rated as following: 1 = severe artefacts, yet diagnostic; 2 = moderate to severe; 3 = minimal to moderate 4 = no artefacts. Background suppression was rated as: 1 = significant background signal, impairing diagnostic validity; 2 = substantial background signal, with significant degradation of image quality; 3 = noticeable background signal, with mild degradation of image quality; 4 = sufficient background suppression, without degradation of image quality. Visualization of biliary and pancreatic ducts: 1 = no or minimal delineation possible; 2 = partial delineation; 3 = delineation of most parts possible; 4 = delineation of the entire ductal structure.

2.4. Quantitative image analysis

Contrast ratios between the common bile duct (CBD) and the adjacent periductal tissue were calculated using following formula:

$$\text{Contrast ratio} = (SI_{CBD} - SI_{periductaltissue})/(SI_{CBD} + SI_{periductaltissue})$$

SI: ROI average signal intensity

CBD: common bile duct

A 5 mm in diameter measuring ROI was placed in die CBD distal to the hepatic duct bifurcation, and in the periductal tissue, sparing bile ducts and areas with motion artefacts.

Additionally, objective quantification of blurring and motion artefacts was performed. Using FIJI's "Line profile" tool [17], a line was manually drawn in the CBD, orthogonal to the longitudinal axis of the duct, at the above-mentioned position. Signal intensities along the line profile were expressed as percentages of the peak intensity inside the CBD. Based on the change per mm at the ductal boundary, a slope profile was calculated.

2.5. Respiratory signal analysis

For both, CRT and BRT datasets the acquired, respiratory signals were recorded by the scanner. Respiratory curves were exported and two respiratory signal quality parameters were extracted to further analyze the impact of the breathing motion on the image quality. The first parameter aimed at the extraction of a respiratory signal SNR metric and was based on the power spectrum of the recorded respiratory signals. Specifically, as a SNR estimate, the area under the curve (AUC) in the breathing range from 0.15 to 0.4 Hz was divided by the AUC of the higher frequency noise contributions above 0.4 Hz. The above breathing range was chosen in such a way that it included all breathing frequency peaks for all patients. The interval below 0.15 Hz was neglected since it contains contributions due to the manufacturer's

DC and gain corrections of the respiratory signal. As the second parameter, the standard deviation of the signal curve during the read-out period was chosen. A low standard deviation value of the respiratory signal during readout was expected to correspond to a successful trigger point determination and less patient movement during data acquisition. Finally, trigger points were visually inspected and false triggering points, i.e. ones that obviously deviate in their position relative to the breathing curve, were counted per exam.

2.6. Statistics

Testing for normal distribution was performed with *D'Agostino-Pearson omnibus K2-test*. A *paired* t-test was used for mean comparison of normally distributed variables, while *Wilcoxon test* was used for variables without normal distribution. The respiratory signal was analyzed using the *Mann-Whitney test*. Inter-observer agreement was calculated using *Cohen´s kappa*. P-values ≤ 0.05 were considered statistically significant.

All statistics were performed using *Prism* Version 7 (*GraphPad* Software) and *IBM SPSS*, version 25.

3. Results

3.1. Qualitative image analysis

3.1.1. Image quality

Overall image quality was compared between belt respiratory triggered (BRT) and camera respiratory triggered (CRT) exams (Figs. 1 and 2). Image quality was superior in CRT compared to BRT datasets (3.20 ± 0.92 vs. 2.84 ± 0.93; P < 0.0001). In detail, poor image quality (Likert scale 1) was only seen in 2 patients (7.1%) in each cohort. Fair image quality (Likert scale 2) was more often seen in BRT (28.6%) compared to CRT (14.3%) exams, whereas good (Likert scale 3) and excellent (Likert scale 4) image quality were seen more often in CRT (35.7% and 46.4%) compared to BRT (32.1% and 28.6%) datasets. *Cohen's kappa* revealed high inter-rater reliability of 0.94 in CRT and 0.95 in BRT.

3.1.2. Blurring and motion artefacts

Significantly less blurring and motion artefacts were noted in CRT examinations compared to BRT examinations (3.29 ± 0.93 vs. 2.91 ± 1.01; P = 0.0020) (Figs. 1 and 2, Table 2). Severe artefacts were seen more frequently in BRT (14.3%) than in CRT (7.1%) exams. Substantially more datasets revealed no artefacts in CRT (57.1%) compared to BRT (32.1%). Inter-reader agreement was 0.88 for CRT and 0.95 for BRT.

3.1.3. Background

Background suppression in CRT examinations was significantly higher compared to BRT examinations (2.64 ± 0.62 vs. 2.54 ± 0.57; P = 0.0326) (Table 2). *Cohen's kappa* was found to be 0.86 for both examinations.

3.1.4. Bile duct visualization

Regarding visualization and image quality of the common bile duct, the left and right hepatic duct, the small hepatic ducts as well as the cystic duct CRT datasets outperformed BRT datasets in all patients (P < 0.0001–0.0013) (Table 2). *Cohen's kappa* revealed high inter-reader agreement for CRT examination (κ = 0.84-0.95) as well as for BRT examinations (κ = 0.85–0.95).

3.1.5. Pancreatic duct visualization

In CRT exams, pancreatic duct visualization and image quality were better compared to BRT (P = 0.003–0.005) (Table 2). High inter-reader agreement was found in both datasets (κ = 0.9–0.95).

3.2. Quantitative image analysis

Acquisition time was 72 s for both sequences. Contrast ratio was significantly higher in CRT (0.94 ± 0.03) than in BRT (0.93 ± 0.03); *paired t*-test P = 0.0017. Analyzing the line profile slope through the CBD revealed significantly higher values in CRT examination (42.23 ± 8.74% of maximum intensity/mm) compared to BRT examination (36.06 ± 8.96% of maximum intensity/mm; *paired* t test p < 0.0001). An example is shown in Fig. 3.

3.3. Respiratory signal analysis

In 7 patients, the rated overall image quality in the CRT datasets was superior to the BRT datasets. The breathing curve signals of these 7

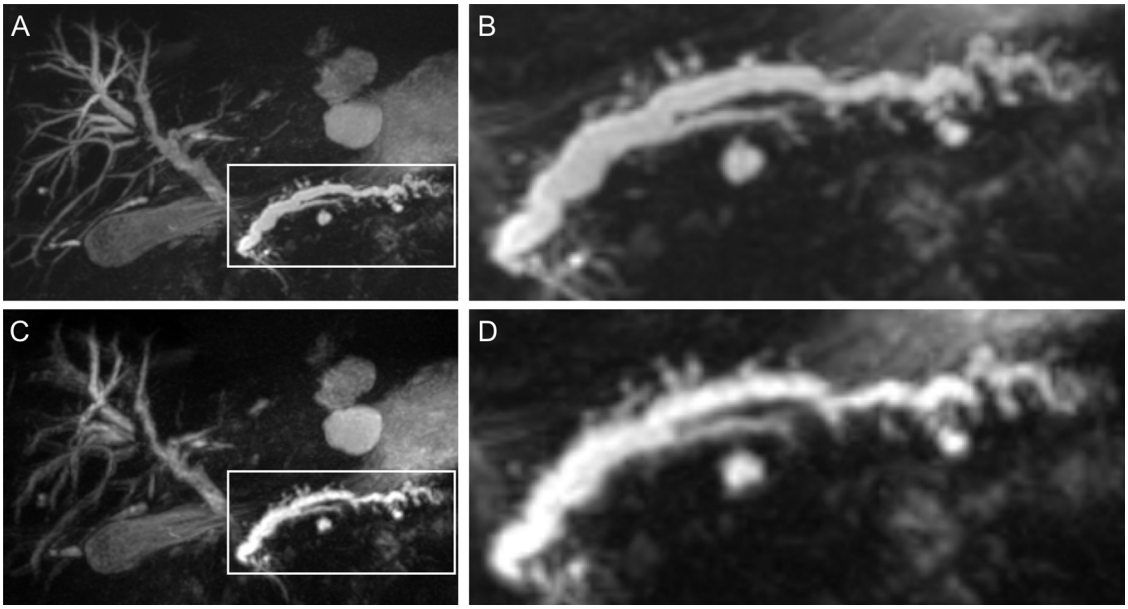

Fig. 1. Patient with multifocal side branch IPMN. The CRT examination (A,B) outperforms the BRT examination (C,D) regarding image quality and blurring.

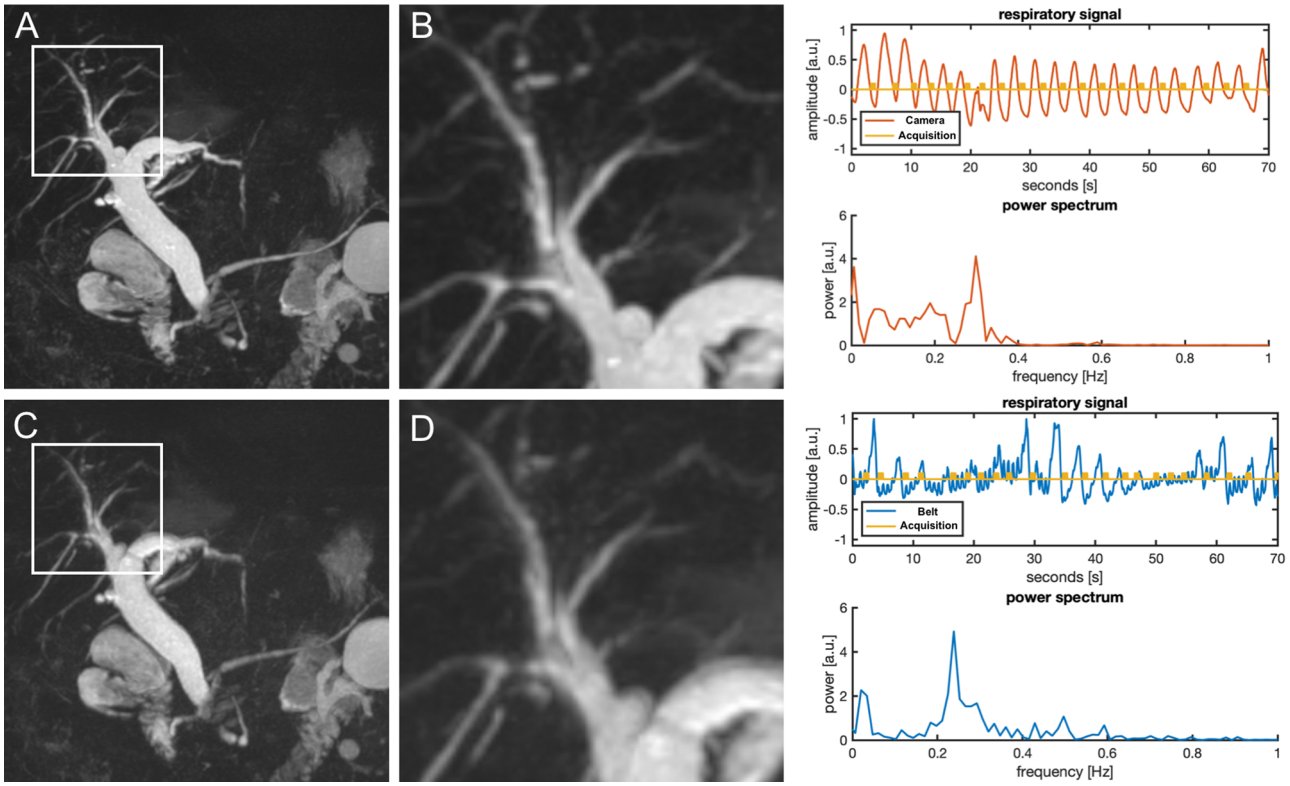

Fig. 2. Enhanced ductal delineation, particularly of the peripheral ducts is seen in CRT datasets (A,B) compared to BRT datasets (C,D). Right column: the corresponding respiratory curves illustrate a more inhomogeneous respiratory signal in BRT datasets (bottom row) compared to CRT (upper row), partially leading to incorrect respiratory triggering.

Table 2
Summary table of all scores for image quality parameters and visualization of the duct structures; values are shown as mean ± standard deviation. P values are given in the right column.

		Respiratory gating		
		Camera	Belt	p
Overall image quality		3.20 ± 0.92	2.84 ± 0.93	< 0.0001
Blurring and motion artefacts		3.29 ± 0.93	2.91 ± 1.01	0.0020
Background suppression		2.64 ± 0.62	2.54 ± 0.57	0.0326
Bile duct visualization	**Common bile duct**	3.38 ± 0.78	3.05 ± 0.72	< 0.0001
	Left hepatic duct	3.16 ± 0.97	2.80 ± 0.92	< 0.0001
	Right hepatic duct	3.13 ± 0.95	2.82 ± 0.90	0.0007
	Anterior branch	3.07 ± 1.01	2.79 ± 0.95	0.0013
	Posterior branch	3.07 ± 1.01	2.77 ± 0.95	0.0007
	Segment 2	2.91 ± 1.16	2.52 ± 1.18	< 0.0001
	Segment 3	2.91 ± 1.13	2.52 ± 1.18	< 0.0001
	Segment 4	2.91 ± 1.13	2.52 ± 1.18	< 0.0001
	Segment 5	2.91 ± 1.13	2.52 ± 1.18	< 0.0001
	Segment 6	2.93 ± 1.14	2.52 ± 1.18	< 0.0001
	Segment 7	2.93 ± 1.14	2.52 ± 1.18	< 0.0001
	Segment 8	2.93 ± 1.14	2.52 ± 1.18	< 0.0001
	Cystic duct	2.98 ± 1.14	2.63 ± 1.04	0.0002
Pancreatic duct visualization	**Proximal**	3.38 ± 0.91	2.96 ± 0.91	0.0005
	Mid	2.93 ± 0.97	2.57 ± 1.08	0.0003
	Distal	2.84 ± 0.99	2.41 ± 1.14	0.0004

patients were compared to the signals of the remaining patients which showed no differing image quality. The AUC ratio was significantly higher for CRT datasets (25.66 ± 12.64) compared to BRT datasets (10.78 ± 8.66) in those 7 patients with superior image quality in CRT examinations (P = 0.0262) (Fig. 4). Furthermore, image quality correlated with the respiratory signal amplitude during the read out. In the above-mentioned 7 patients, a lower standard deviation was seen in CRT datasets (0.11 ± 0.004) compared to BRT datasets (0.20 ± 0.14) without reaching statistical significance (P = 0.1375). A comparable signal amplitude was found in the remaining patients (0.12 ± 0.05 in CRT vs. 0.11 ± 0.05 in BRT, P = 0.5161) (Fig. 4). Visual analysis of the exported breathing curves (Fig. 2) revealed fewer false triggers in CRT-MRCP in the group with improved image quality (2.7 ± 2.9) and no significant variation among the remaining patients (0.5 ± 3.0).

4. Discussion

In our study, we compared the performance of a novel, camera-

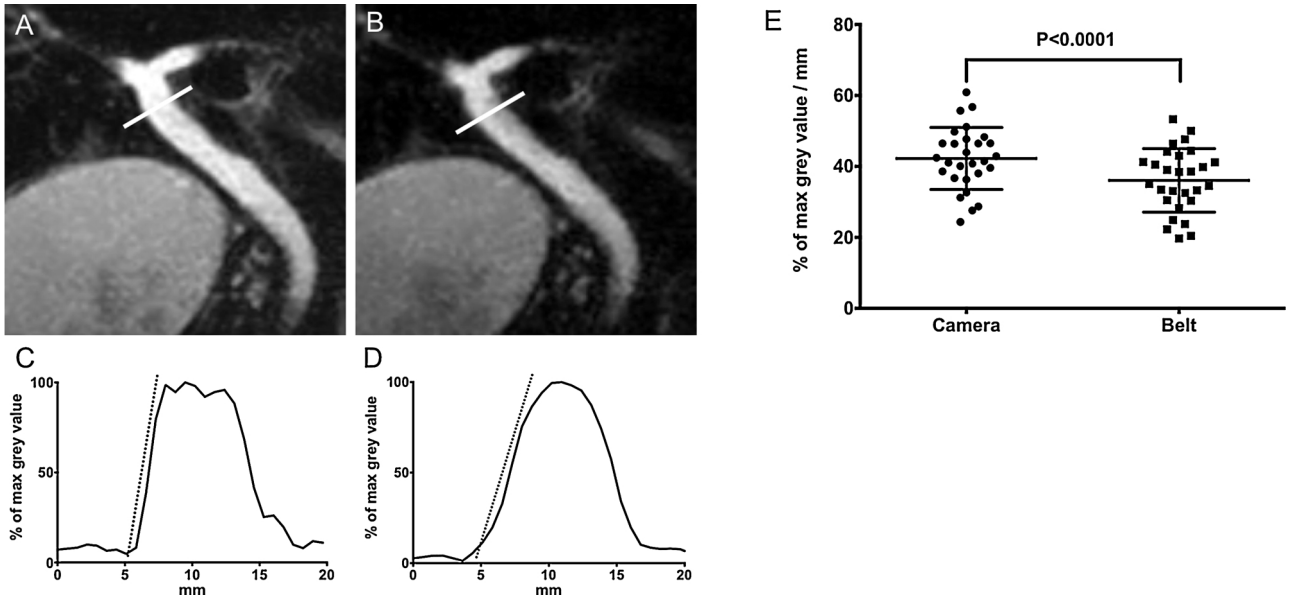

Fig. 3. Depiction of line profile slopes through the CBD for CRT (A, C) and BRT (B, D) examinations. Overall significantly higher slope values were found for CRT datasets. (E).

based (CRT) to a conventional belt-based (BRT) respiratory triggering approach in 3D-MRCP and found the CRT approach to provide higher image quality, which we attribute to an improved respiratory signal curve and more reliable timing of the triggered acquisition.

The lower spatial resolution and signal intensity of single shot 2D and breath-hold 3D MRCP acquisitions can obscure small pathologies in the evaluation of the pancreatobiliary tree (PBT) [18]. In contrast, the potential benefit of higher spatial resolution and signal intensity of navigator- or respiratory-triggered 3D MRCP are often nullified by motion artefacts.

Accelerated image acquisition using compressed sensing, has significantly improved image quality in respiratory-triggered 3D MRCP sequences [7,19,20]. However, even with such fast imaging techniques in place, image quality can be severely affected in patients that exhibit irregular breathing patterns, which translate into variation in breathing curves, trigger points of the individual acquisition steps in relation to organ position and potentially even data acquisition during major organ motion.

We applied a compressed sensing (CS) accelerated 3D MRCP-sequence with CS-factor 15, resulting in a total acquisition time of 72 s, irrespective of the applied triggering approach. Despite this short acquisition time, a small subset of exams was of poor image quality, exhibiting artefacts from motion and blurring or insufficient background suppression. Whereas CRT MRCP did not prevent such cases from occurring, mean image quality was significantly better compared to BRT.

Concurrently respiratory triggering is mainly performed using either additional navigator MR signals or external devices such as respiratory belts. Navigator MR signals provide motion compensation but depend on the quality of the acquired pencil beam navigator and require pulse sequence modifications [21]. The application of respiratory belts can be limited due to its user dependency and its additional workload. Furthermore, correct belt and navigator placement is dependent on the breathing type of each patient, which is not always easy to determine. In addition to that, respiratory belts can become unreliable when motion artefacts result from the delay between alteration in the thoracic diameter and motion of the diaphragm [21].

Previously reported studies introduced the implementation of camera-based motion detection in MRI. However, up to now research is focused particularly on musculoskeletal MRI and functional MRI of the brain [11,13,22]. Yet musculoskeletal imaging as well as imaging of the brain are considerably less motion-sensitive than abdominal imaging. Furthermore, previous studies focusing on camera-based triggering additionally used external devices such as markers attached to the surface, which again require a technician to prepare the patients, resulting in an increased examination time [15,22]. Best to our knowledge only one previous study investigated camera-based abdominal motion triggering, yet focusing on HIFU [23].

In our study, we found significantly higher overall image quality in camera respiratory triggered examinations (CRT). Regarding ductal delineation of the PBT, CRT significantly outperformed belt respiratory triggered examinations (BRT). Particularly in distal ductal segments, such as the S2-4 of the left hepatic duct, S5-8 of the right hepatic ducts as well as the mid and distal part of the pancreatic duct, superiority of CRT was seen. This is an important finding, indicating that CRT might improve diagnostic validity in diseases which may predominantly be located in small ducts of the PBT, e.g. primary sclerosing cholangitis or primary biliary cholangitis [24,25]. Furthermore, significantly less blurring and motion artefacts were seen in CRT. This subjective finding was supported by analysis of the line slope profiles which were significantly higher in CRT compared to BRT datasets. Additionally, our findings were supported by the analysis of the respiratory signal curves acquired for both, the CRT and BRT datasets respectively.

Our study has some limitations. Most important the relatively small sample size has to be mentioned. However, showing significantly better results in CRT compared to BRT datasets in all qualitative and quantitative parameters, we believe our results to be robust. We did not correlate our findings to diagnosis made in MRCP, since our aim was to investigate technical feasibility of CRT in 3D MRCP. This study was performed on a 3 T system. Our results may not be generalized using other field strengths. In addition to that, our findings should be investigated in further studies regarding specific pancreatobiliary diseases.

In conclusion, our study proved superiority of CRT over BRT in CS-accelerated 3D MRCP regarding image quality, artefacts and ductal delineation for the first time.

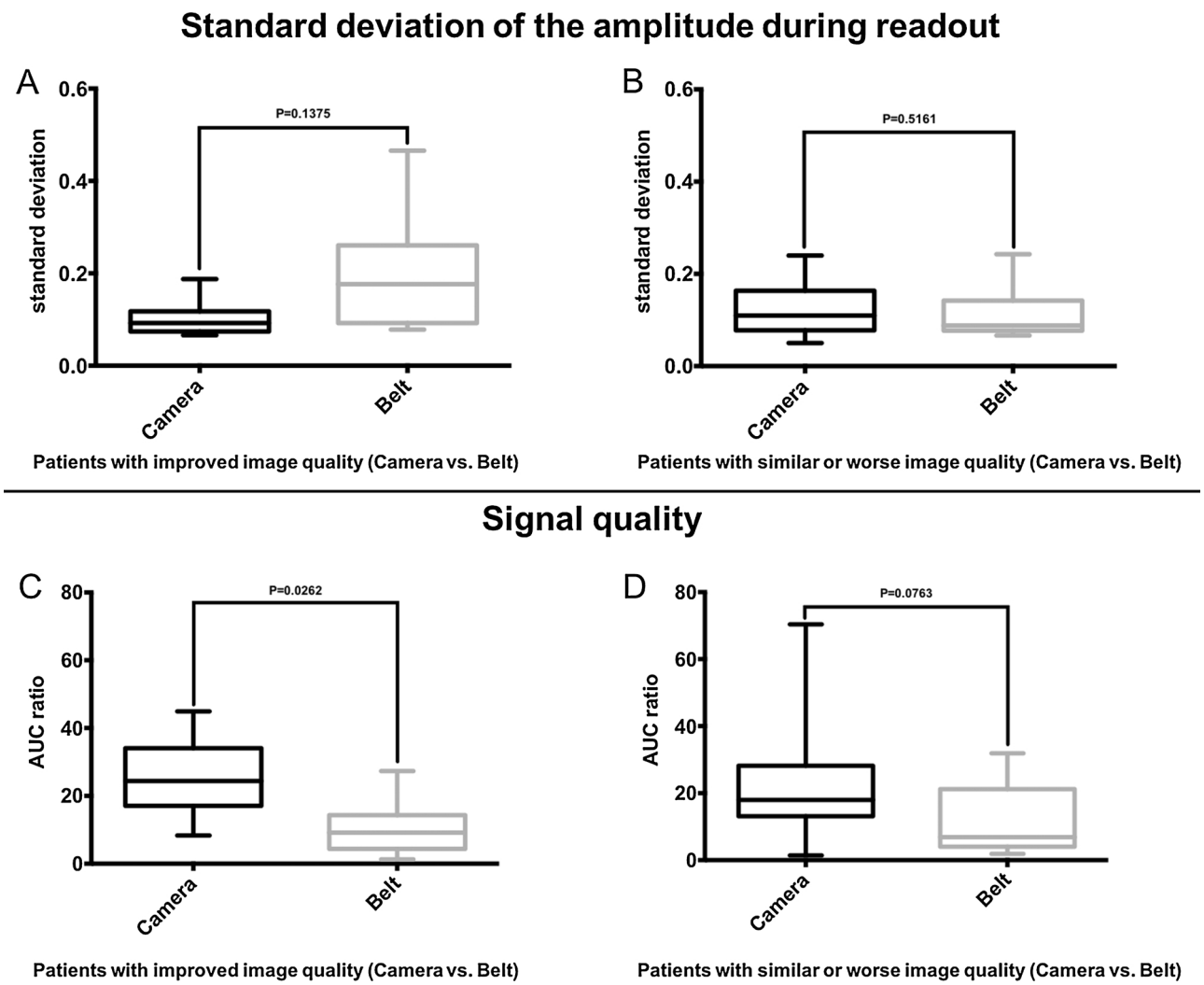

Fig. 4. The standard deviation of the amplitude during the readout of the respiratory signal is shown in patients with improved image quality (Camera vs. Belt) (A) and patients with similar or worse image quality (Camera vs. Belt) (B). Signal quality of the respiratory signal is shown as AUC ratio in patients with improved image quality (Camera vs. Belt) (C) and patients with similar or worse image quality (Camera vs. Belt) (D). AUC ratio was significantly higher in CRT compared to BRT in patients with improved image quality (C), P = 0.0262).

Conflict of interest

The authors acknowledge research support from Philips Healthcare.

Funding

The authors state that this work has not received any funding.

Ethical approval

Institutional Review Board approval was obtained.

References

[1] N. Griffin, G. Charles-Edwards, L.A. Grant, Magnetic resonance cholangiopancreatography: the ABC of MRCP, Insights Imaging 3 (1) (2012) 11–21.
[2] D.H. Park, M.H. Kim, S.S. Lee, S.K. Lee, K.P. Kim, J.M. Han, S.Y. Kim, M.H. Song, D.W. Seo, A.Y. Kim, T.K. Kim, Y.I. Min, Accuracy of magnetic resonance cholangiopancreatography for locating hepatolithiasis and detecting accompanying biliary strictures, Endoscopy 36 (11) (2004) 987–992.
[3] M.S. Park, T.K. Kim, K.W. Kim, S.W. Park, J.K. Lee, J.S. Kim, J.H. Lee, K.A. Kim, A.Y. Kim, P.N. Kim, M.G. Lee, H.K. Ha, Differentiation of extrahepatic bile duct cholangiocarcinoma from benign stricture: findings at MRCP versus ERCP, Radiology 233 (1) (2004) 234–240.
[4] P. Pavone, A. Laghi, C. Catalano, L. Broglia, V. Panebianco, A. Messina, F.M. Salvatori, R. Passariello, MR cholangiography in the examination of patients with biliary-enteric anastomoses, AJR Am. J. Roentgenol. 169 (3) (1997) 807–811.
[5] M.G. Lee, H.J. Lee, M.H. Kim, E.M. Kang, Y.H. Kim, S.G. Lee, P.N. Kim, H.K. Ha, Y.H. Auh, Extrahepatic biliary diseases: 3D MR cholangiopancreatography compared with endoscopic retrograde cholangiopancreatography, Radiology 202 (3) (1997) 663–669.
[6] J.H. Lee, S.S. Lee, J.Y. Kim, I.S. Kim, J.H. Byun, S.H. Park, M.G. Lee, Parallel imaging improves the image quality and duct visibility of breathhold two-dimensional thick-slab MR cholangiopancreatography, J. Magn. Reson. Imaging 39 (2) (2014) 269–275.
[7] F.K. Lohöfer, G.A. Kaissis, M. Rasper, C. Katemann, A. Hock, J.M. Peeters, C. Schlag, E.J. Rummeny, D. Karampinos, R.F. Braren, Magnetic Resonance Cholangiopancreatography at 3 Tesla: image quality comparison between 3D compressed sensing and 2D single-shot acquisitions, Eur. J. Radiol. (2019), https://doi.org/10.1016/j.ejrad.2019.04.002 In press.
[8] M. Yoshida, T. Nakaura, T. Inoue, S. Tanoue, S. Takada, D. Utsunomiya, S. Tsumagari, K. Harada, Y. Yamashita, Magnetic resonance cholangiopancreatography with GRASE sequence at 3.0T: does it improve image quality and acquisition time as compared with 3D TSE? Eur. Radiol. 28 (6) (2018) 2436–2443.
[9] L. Zhu, X. Wu, Z. Sun, Z. Jin, E. Weiland, E. Raithel, T. Qian, H. Xue, Compressed-sensing accelerated 3-Dimensional magnetic resonance cholangiopancreatography: application in suspected pancreatic diseases, Invest. Radiol. 53 (3) (2018) 150–157.
[10] R.L. Ehman, M.T. McNamara, M. Pallack, H. Hricak, C.B. Higgins, Magnetic resonance imaging with respiratory gating: techniques and advantages, AJR Am. J. Roentgenol. 143 (6) (1984) 1175–1182.
[11] S.A. Chikop, A.B.S. Anchan, G. Koulagi, A.A. Honnedevasthana, S. Imam, S. Geethanath, Automatic motion correction of Musculoskeletal MRI using DSLR camera, Magn. Reson. Imaging 48 (2018) 74–79.
[12] T. Lange, J. Maclaren, M. Herbst, C. Lovell-Smith, K. Izadpanah, M. Zaitsev, Knee cartilage MRI with in situ mechanical loading using prospective motion correction,

Magn. Reson. Med. 71 (2) (2014) 516–523.
[13] J. Maclaren, M. Aksoy, M.B. Ooi, B. Zahneisen, R. Bammer, Prospective motion correction using coil-mounted cameras: cross-calibration considerations, Magn. Reson. Med. 79 (4) (2018) 1911–1921.
[14] D. Maziero, T.R. Velasco, N. Hunt, E. Payne, L. Lemieux, C.E.G. Salmon, D.W. Carmichael, Towards motion insensitive EEG-fMRI: correcting motion-induced voltages and gradient artefact instability in EEG using an fMRI prospective motion correction (PMC) system, NeuroImage 138 (2016) 13–27.
[15] N. Todd, O. Josephs, M.F. Callaghan, A. Lutti, N. Weiskopf, Prospective motion correction of 3D echo-planar imaging data for functional MRI using optical tracking, NeuroImage 113 (2015) 1–12.
[16] M. Rocque, Fully automated contactless respiration monitoring using a camera, 2016 IEEE International Conference on Consumer Electronics (ICCE) (2016).
[17] J. Schindelin, I. Arganda-Carreras, E. Frise, V. Kaynig, M. Longair, T. Pietzsch, S. Preibisch, C. Rueden, S. Saalfeld, B. Schmid, J.Y. Tinevez, D.J. White, V. Hartenstein, K. Eliceiri, P. Tomancak, A. Cardona, Fiji: an open-source platform for biological-image analysis, Nat. Methods 9 (7) (2012) 676–682.
[18] J.F. Glockner, M. Saranathan, E. Bayram, C.U. Lee, Breath-held MR cholangiopancreatography (MRCP) using a 3D Dixon fat-water separated balanced steady state free precession sequence, Magn. Reson. Imaging 31 (8) (2013) 1263–1270.
[19] J. Taron, J. Weiss, M. Notohamiprodjo, T. Kuestner, F. Bamberg, E. Weiland, B. Kuehn, P. Martirosian, Acceleration of magnetic resonance cholangiopancreatography using compressed sensing at 1.5 and 3 t: a clinical feasibility study, Invest. Radiol. 53 (11) (2018) 681–688.
[20] J.H. Yoon, S.M. Lee, H.J. Kang, E. Weiland, E. Raithel, Y. Son, B. Kiefer, J.M. Lee, Clinical feasibility of 3-Dimensional magnetic resonance cholangiopancreatography using compressed sensing: comparison of image quality and diagnostic performance, Invest. Radiol. 52 (10) (2017) 612–619.
[21] Z.A. Ćeličanin, Respiratory Organ Motion in Interventional MRI: Tracking, Guiding and Modeling, Basel University, 2016.
[22] J. Maclaren, M. Aksoy, R. Bammer, Contact-free physiological monitoring using a markerless optical system, Magn. Reson. Med. 74 (2) (2015) 571–577.
[23] V. Auboiroux, L. Petrusca, M. Viallon, A. Muller, S. Terraz, R. Breguet, X. Montet, C.D. Becker, R. Salomir, Respiratory-gated MRgHIFU in upper abdomen using an MR-compatible in-bore digital camera, Biomed Res. Int. 2014 (2014) 421726.
[24] V.I. Reshetnyak, Primary biliary cirrhosis: clinical and laboratory criteria for its diagnosis, World J. Gastroenterol. 21 (25) (2015) 7683–7708.
[25] K.N. Lazaridis, N.F. LaRusso, Primary sclerosing cholangitis, N. Engl. J. Med. 375 (12) (2016) 1161–1170.